Effect of vortical structures on cavitation on impeller blades in pumps with suction chambers

A Škerlavaj[1] and R Pavlin[2]

[1] Department for Basic Research and Education, Turboinštitut, Rovšnikova 7, 1000 Ljubljana, Slovenia

[2] Pumps Programme, Turboinštitut, Rovšnikova 7, 1000 Ljubljana, Slovenia

E-mail: aljaz.skerlavaj@turboinstitut.si

Abstract. A double-suction pump operating at relatively low suction head and with poorly designed suction chambers was analysed by the computational fluid dynamics (CFD). Two impeller geometries were considered - one with thicker and one with thin layer of predicted vapour cavity on blades. Steady-state simulations (SSS) were performed with shear-stress-transport (SST) turbulence model with curvature correction (CC). Transient simulations were performed with scale-adaptive-simulation SST (SAS-SST) model with CC. For both analysed geometries, transient simulations predicted higher maximal thickness of cavities than SSS. In transient simulations it was observed that, because of poor design of suction chambers, near the rib of the suction chambers two stronger (non-cavitating) vortices appeared. Near the main vortical structures, vortices with smaller intensity appeared, with direction of rotation opposite to the main vortices. Depending on their position and direction of rotation, the vortices either decreased or increased the extent of cavitation. The most important adverse effect was to increase the size of the sheet cavity by local elongation and thickening. The local effect seemed to be more pronounced for impeller with smaller thickness of sheet cavity.

1. Introduction

It is well known that an improperly designed suction chamber or pump sump can be a reason for appearance of cavitating vortices (also called vortex ropes) in various pumps. In case of radial-flow rotodynamic pumps, the suction chamber may cause cavitating vortices in double-suction pumps or in the first stage of multi-stage (single-suction) pumps. In case of vertical mixed-flow and axial-flow rotodynamic pumps, the improperly designed pump sump is a reason for (cavitating or non-cavitating) vortices entering the impeller. In case of jet (ejector) pumps, cavitating vortices in secondary (suction) fluid may appear because of flow of secondary fluid inside the suction chamber past the (main) pipe that ends with the nozzle.

In case of rotodynamic pumps, such cavitating vortices are cut by the impeller blades. This was clearly presented by Sato et al. [1], as well as the force exerted on the impeller by the collapse of the cut piece of the cavitating vortex. They can cause vibrations and, as reported in [2], material damage on pressure side. The cavitating vortices can be detected by performing pump model tests.

In this paper, an effect (not previously known to authors) of non-cavitating vortices on the cavitation on impeller is presented. Such vortices cannot be observed in experimental model tests but

Content from this work may be used under the terms of the Creative Commons Attribution 3.0 licence. Any further distribution of this work must maintain attribution to the author(s) and the title of the work, journal citation and DOI.
Published under licence by IOP Publishing Ltd

it may be possible to see their effect – stretched cavity of vapour on impeller blade near the rib of the suction chamber.

A double-suction pump with rather low suction head was refurbished. Because of low head, the pump is prone to cavitation problems. Besides, suction chambers were designed in the 1960's. They were found inappropriate for the pump because of non-evenly decreasing area of its cross-sections. Because of poorly designed suction chambers, vortices appear near the rib of the chamber. The pump is of small importance in the complex hydropower system. Thus, only small modifications were allowed – only the impeller could be changed and the model testing could not be performed. Cavitating problems with 'original' design and the result of the modification of the impeller (the modification is denoted as Geometry 1 in this paper) were described in [3]. The second modification for the 'spare' impeller (marked as Geometry 2), where an interference between (thin) sheet cavitation and strong vortices resulted in either locally increased or reduced cavitation extent, is presented in this paper.

2. Numerical method

Numerical simulations were performed using a finite-volume commercial solver ANSYS CFX [4] at LSC Adria supercomputing centre. The centre is located at Turboinštitut and consists of 256 IBM HS22 blade servers, each equipped with two quad-core Intel Xeon processors L5530 2.4GHz 8MB L2 and 16 GB RAM. For fast inter-node communication the Infiniband link with MPI protocol is used.

Computational domain (figure 1) consists of three unstructured computational meshes with hexa-cores, similar to numerical setup presented in [3]. Meshes were created for piping with suction chambers, for impeller, and for spiral casing with diffuser. Table 1 presents mesh sizes for final geometry (Geometry 2), whereas some meshing details are presented in figure 2. For consistency reasons between this paper and our previous paper [3], number of nodes in meshes of Geometry 1 is the same as in [3] (roughly half the ones of Geometry 2). Nevertheless, simulations were performed also with the same mesh density as presented in Table 1 and results were similar. For all geometries and for both mesh densities the average value of y^+ in the impeller was around 80.

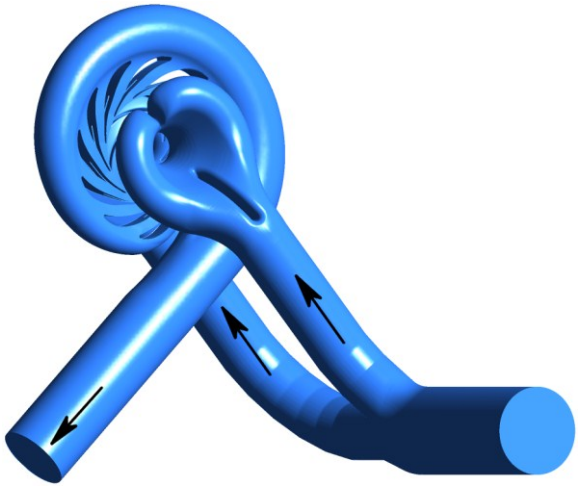

Figure 1. Computational domain of the pump. Arrows show flow direction.

Table 1. Sizes of computational meshes (for Geometry 2).

Computational mesh	Number of elements	Number of nodes
Piping with suction chambers	14,622,385	6,855,330
Impeller (both sides)	19,094,978	7,922,894
Diffuser and spiral casing	6,334,592	2,238,219
Total	40,051,955	17,016,443

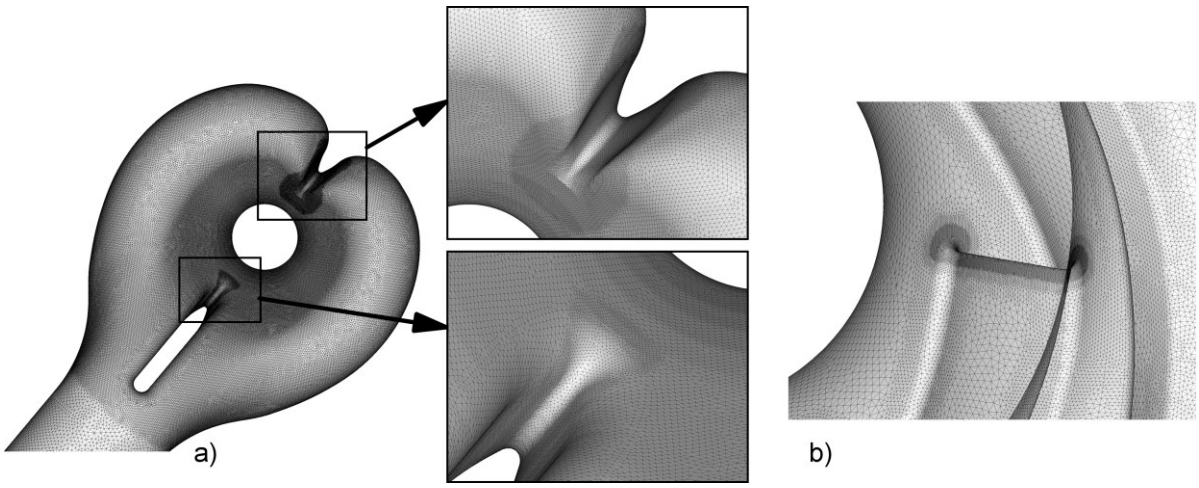

Figure 2. Details of computational mesh: (a) Suction chambers and (b) impeller blade leading edge.

The simulations were performed for the prototype size of the storage pump. Steady-state simulations with the shear-stress-transport turbulence model [5] with curvature correction [6] (SST-CC) resulted in about eight per cent too high pump head (for Geometry 1) [3, 7]. Torque was more than 20% too high. Results of transient simulations performed with the scale-adaptive-simulation shear-stress-transport turbulence model [8] with curvature correction (SAS-SST-CC) were close to the measured values. Therefore, the SAS-SST-CC turbulence model was used also for final predictions of Geometry 2.

Numerical setup of simulations of Geometry 1 was already presented in [3], so only the setup for Geometry 2 is presented (it is very similar to the one for Geometry 1). Steady-state simulations (for Geometry 2) were performed with the local time-scale factor equal to ten for 1500 iterations with the cavitation model being used. A transient simulation was performed with time step equal to 2 degrees of impeller rotation and started from steady-state solution. It lasted for 33 impeller revolutions without the cavitation model and for eight revolutions with the cavitation model. Courant number was equal to five. Number of iterations per time step was limited to six. This condition resulted in the maximum residuals being below 8.3×10^{-2} and the RMS residuals below 3.5×10^{-4}.

Results of the transient simulation for Geometry 2 were verified with a transient simulation with smaller time-step size. The second transient simulation continued from the result of the first transient simulation (with the cavitation model). The time-step size corresponded to 0.4 degree of impeller rotation and the simulation time corresponded to one impeller revolution. In the second simulation, the RMS Courant number was around one. The maximum residuals were below 7×10^{-2}, whereas the RMS residuals were below 2.1×10^{-4}. Results (predicted size of vapour cavities on blades) of the second simulation were similar to previous ones (with 2° time step).

Total pressure condition was used at the inlet boundary and mass flow rate was specified at outlet. Where effects of labyrinth seals were taken into account, flow rate through labyrinth seals was assumed to be equal to 3% of nominal flow rate. Nominal flow rate was equal to 2 m^3/s. The labyrinth seals were modelled with outlet and inlet mass flow boundary conditions at rings (thin surfaces) just before and after the impeller.

In steady-state simulations the 'high-resolution' advection scheme was used, which is an upwind adaptive scheme, based on the Barth and Jespersen's limiter [9], and assures the boundedness of the solution. In transient simulations a bounded central-difference scheme was used, which is based on the normalised variable diagram. It blends from the central difference scheme (CDS) to the first-order upwind scheme when the convection boundedness criterion [10] is violated. The second-order backward Euler transient scheme was used as a time-stepping scheme in transient simulations. The cavitation model used was already described in [3]. The model is based on a Rayleigh-Plesset

equation. Default values of cavitation condensation and vaporisation coefficients were used (0.01 and 50, respectively).

3. Results

Results of numerical simulations are presented for Geometry 1 and 2, for both types of numerical simulations: steady-state SST-CC and (transient) SAS-SST-CC (figures 3 to 7).

In case of Geometry 1, the transient simulation resulted in overall thicker sheet cavities than the ones obtained with steady-state SST-CC simulation (figure 3). Besides thickness, there is no other (obvious) difference in cavities (e.g., shape or length). In transient simulation, two cavities were somewhat thicker than the others. Because fluid flow in inlet casings is divided in two halves when it flows towards the rib, Gülich [2] describes that it has either pre-rotating (PR) or counter-rotating (CR) effect (relative to the rotation direction of the impeller). Fluid impinges at rib, which near hub results in counter-flow to the general direction of fluid in suction chambers. It can be concluded that a situation near the rib of suction chambers can be quite complex.

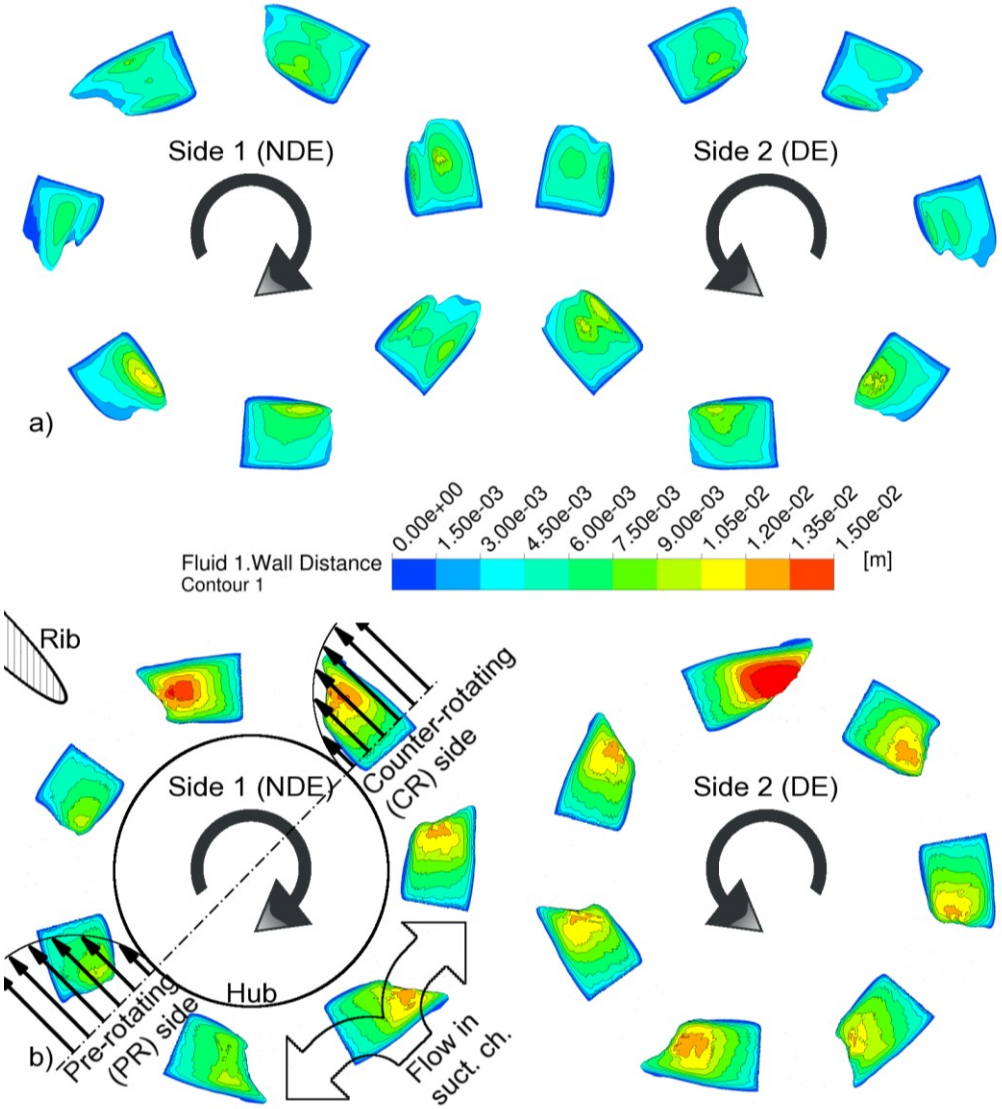

Figure 3. Cavitation on impeller for Geometry 1: isosurface of 1% vapour, coloured by wall distance. (a) steady-state SST-CC; (b) SAS-SST-CC. NDE: non-drive end. DE: drive end. Scheme added into (b): division of flow in suction chambers, rib, hub and flow velocity profiles in suction chamber.

A simplified flow situation in suction chambers is presented schematically in Fig. 3b for the NDE side (for DE side a horizontally flipped situation applies). It can be observed that thickness of sheet cavities is increased at a counter-rotation inflow side (and decreased at a pre-rotation inflow side). Change of velocity triangle for the CR inflow effect is presented in figure 4 – relative velocity w_1 increases, which means that flow angle β_1 (between w_1 and u_1) decreases. This results in increased cavity size on suction side of impeller blade (figure 4b). The effect of the PR or CR flow on the thickness of sheet cavities could also be observed in case of original impeller geometry [3].

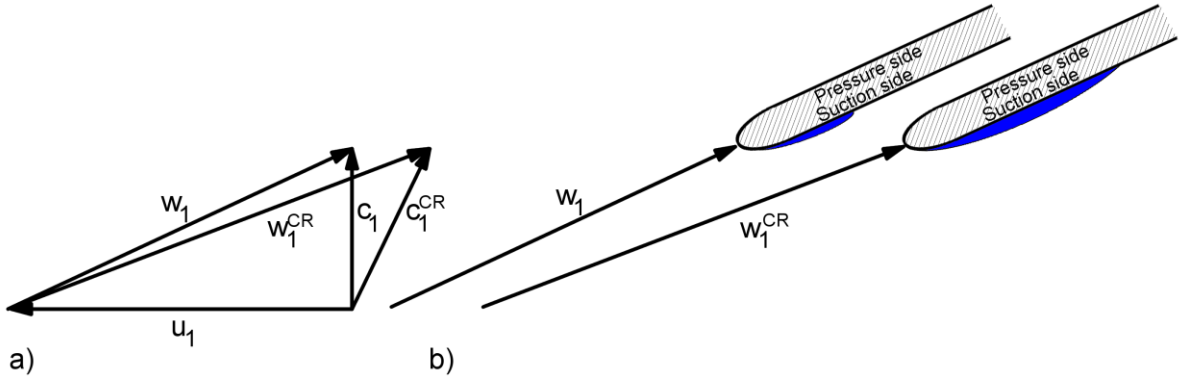

Figure 4. Counter-rotation (CR) effect of fluid in inlet chamber on: (a) velocity triangle at pump impeller leading edge; (b) increased sheet cavity on suction side of impeller blade due to changed angle of attack of w_1.

In case of Geometry 2, overall thickness of sheet cavities is much smaller than in case of Geometry 1, for both types of simulations (figure 5). Thickness of cavities is smaller in transient than in steady-state simulation, which is a consequence of increased flow through impeller (for 3% of nominal flow) due to labyrinth seals. Labyrinth seals were not considered in case of steady-state simulation. On one of the blades at NDE side (marked with red ellipse in figure 5b) the sheet cavity is much larger than on all other blades. The cavity is thicker and longer than others, but only near the shroud. The reason for such behaviour is a presence of strong vortex in inlet casing, as presented in figure 6.

In figure 6a, it can be observed that near the rib of the suction chamber two stronger vortices (indicated with A and C) appear on each side of the rib, which rotate in opposite directions. Their position is in agreement with Gülich [2]. In vicinity of the main vortical structures (A and C), vortices with smaller intensity appear. Direction of their rotation is opposite to rotation of the nearest strong vortex. An example is vortex B, which is rotating next to vortex A. There is a similar (but hardly visible) vortex next to vortex C. Visibility of vortices depends on chosen value of second invariant of velocity gradient [11] Q, as well as on mesh density. Large-sized elements tend to diffuse the vortex strength. Vortices in the suction chambers appeared in simulations with original geometry of the impeller, with Geometry 1 and with Geometry 2. Although we tried to eliminate vortices during the early stage of the project, there was no evidence the vortices affected the flow of original impeller and Geometry 1. After the flow in a pump was observed through a special plexi-glas window [3] and no sign of cavitating vortices was found, the ideas about possible small modifications of the suction chambers were abandoned.

In case of Geometry 2, the results of the transient simulation (figure 6) show that (non-cavitating) vortices locally affect the cavities. Depending on position and direction of rotation, the vortices either decrease or increase the extent of cavitation. The most important adverse effect is to increase the size of the sheet cavity by local elongation and thickening of the sheet. For instance, in figure 6a the vortex A increases the size of sheet cavity on blade 1 by increasing relative velocity of fluid over the suction side of impeller blade near shroud. After blade 1 passes the main vortex (figures 6b to 6f), size of the cavity slowly decreases. In figure 6a, size of sheet cavity on blade 2 is small. Blade 2 approaches vortex B in figure 6b. Because the vortex rotates in opposite direction to vortex A, relative velocity of

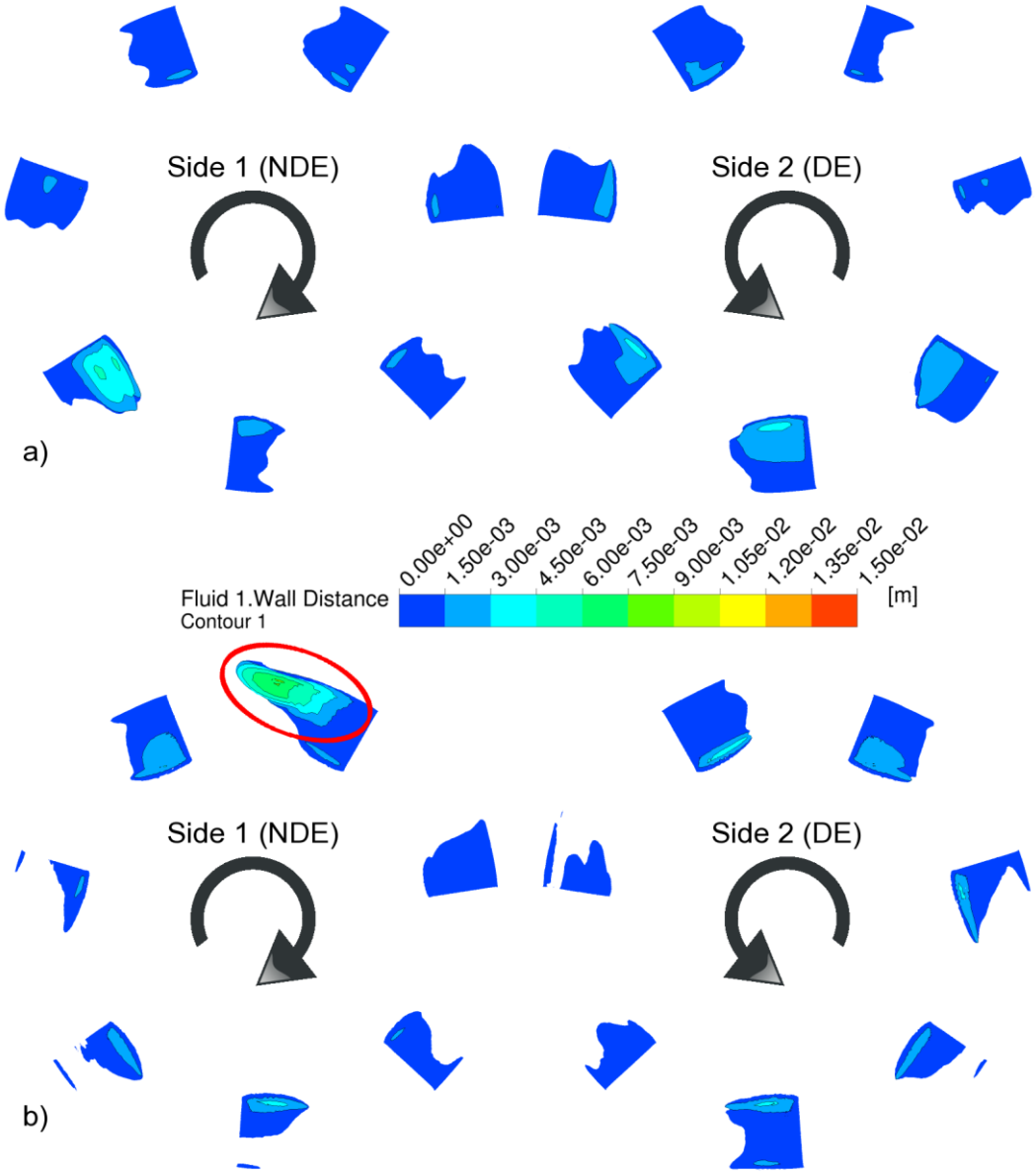

Figure 5. Cavitation on impeller for Geometry 2: isosurface of 1% vapour, coloured by wall distance. (a) steady-state SST-CC; (b) SAS-SST-CC. NDE: non-drive end. DE: drive end.

fluid over suction side of blade near shroud is decreased. This results in area without cavitation on leading edge of blade 2, close to the shroud. With impeller rotation, as the blade 2 moves past the vortex B, the non-cavitating area on blade 2 moves from leading edge towards the back of the blade. In figure 6c the part without cavitation on blade 2 (near shroud) penetrates from the end of the cavity almost to the leading edge. In figure 6d, there is no effect of vortex B on sheet cavity on blade 2. The size of the cavity starts to increase due to influence of vortex A. In figure 6e, the size of cavity on blade 2 is further increased, which continues in figure 6f. Position of blade 2 in figure 6f is the same as position of blade 1 in figure 6a.

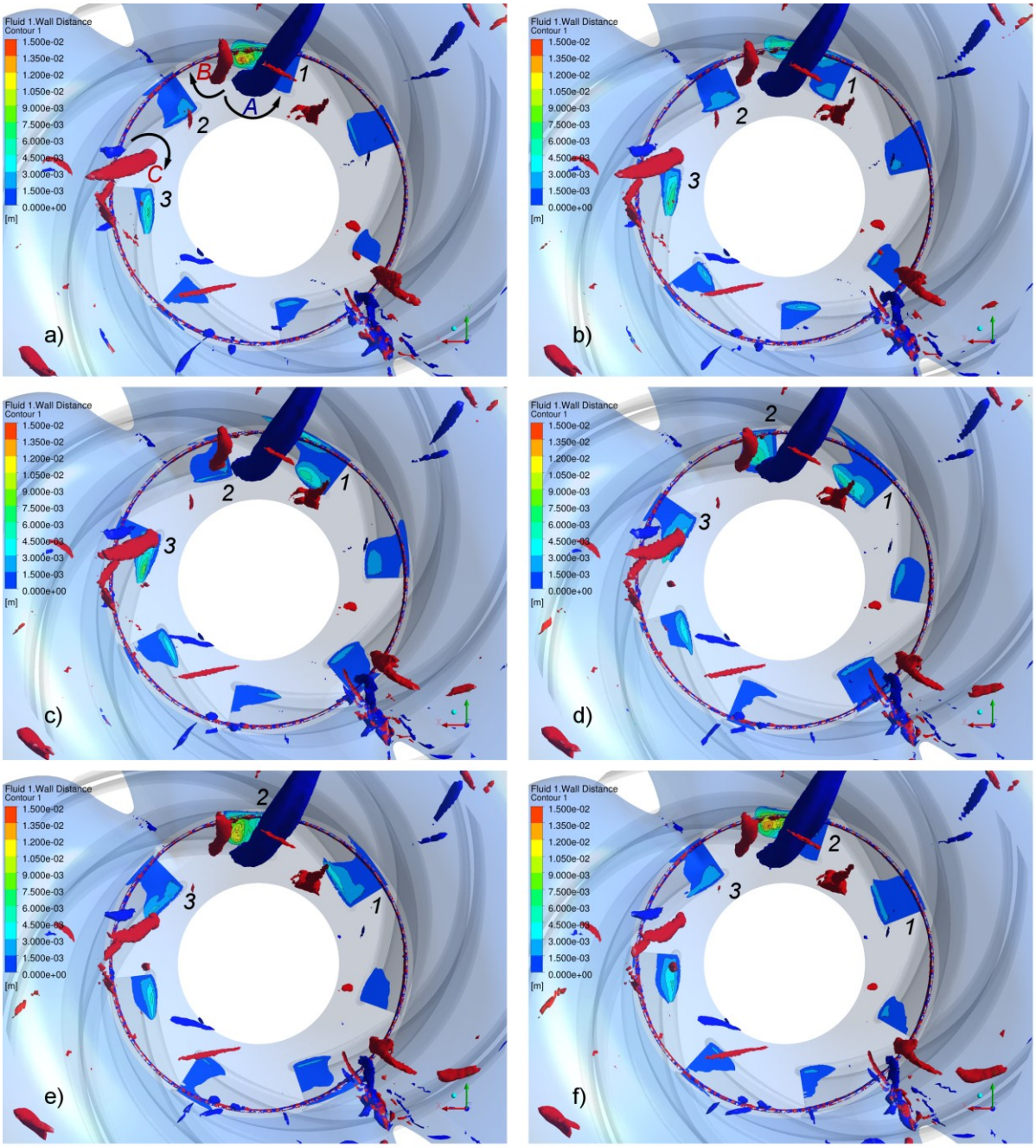

Figure 6. Result of SAS-SST-CC: sheet cavities (1% of water vapour, coloured by wall distance) and vortical structures (second invariant of velocity gradient [11] Q=30,000 s^{-2}) in NDE of Geometry 2. (a) to (f) represent sequential rotations of an impeller for 10.29°. Numbers mark impeller blades. Colours of vortices represent direction of rotation (swirling vector Z).

Steady-state simulations did not predict stretched sheet cavities. It is assumed that stretched cavities (which occur due to strong vortices in suction chambers) can also lead to local cloud cavitation. In our related paper [3] it was shown that cloud cavitation was not predicted by CFD.

The relative importance of effect of vortices seemed smaller for Geometry 1 than for Geometry 2. In case of Geometry 1, maximal thickness of sheet cavities at CR side, except for the blade close to the rib, is around 1.3 cm (figure 3b). In case of Geometry 2, such thickness (away from hub) is below 1.5

mm (figure 5b). Figure 7a depicts maximal thickness of sheet cavities (over all blades) versus radius. The largest thickness of cavity for Geometry 1 and for Geometry 2 is equal to 2.13 cm and 0.81 cm, respectively. Therefore, maximal thickness of cavity at the blade close to the rib, relative to maximal thickness of other cavities at CR side, is for Geometry 1 and Geometry 2 roughly equal to 160% and 540%, respectively. Although it could not be concluded that the main reason for the thickest cavities in case of Geometry 1 were vortices, such effect is smaller than the effect of vortices in case of Geometry 2.

Position of appearance of maximal thickness of cavities (figure 7a) was different between the two geometries. Compared to the steady-state simulation, the transient simulation of Geometry 1 increased thickness at mid-span between hub and shroud. In case of Geometry 2, transient simulation increased the maximal thickness near shroud (large radius) - due to effect of vortices. For both geometries, the peak moved towards larger radius when comparing transient simulations to steady-state results.

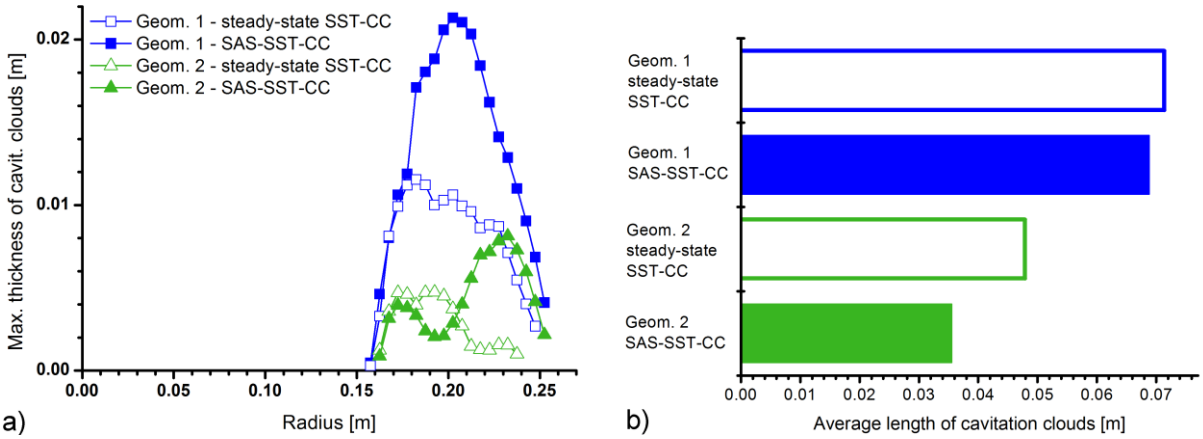

Figure 7. Prediction of (a) maximal thickness of sheet cavities versus radius; (b) average length of cavities.

Figure 7b depicts average length of cavities (calculated as area of top surfaces of sheet cavities, divided by width of cavities, and averaged over all blades). In case of Geometry 1, difference between steady-state and transient simulation was small. In case of Geometry 2, average cavity predicted with transient simulation was around 20% shorter than a cavity predicted with steady-state simulation. The reason is attributed to 3% increased flow through impeller due to labyrinth seals. Such conclusion is based on effect of 10% increased flow rate in steady-state simulations. In graph 7b it is not obvious that in case of Geometry 2 there was large difference between transient and steady-state simulations in local length of sheet cavities.

4. Summary and conclusions

In two presented cases, transient simulations predicted larger maximal thickness of sheet cavities on impeller blades of double-suction centrifugal pump than the steady-state simulations. In case of Geometry 2, the cavitation sheet was thin in general, but strong vortices that formed near rib of suction chambers locally increased or reduced the cavity near shroud. As a result, presence of strong vortices can shorten the lifetime of the impeller. The local effect was more pronounced for impeller with thinner sheet cavities.

Based on our simulation of floor vortex in pump intakes [12], where good agreement was obtained between the SAS-SST-CC simulation and experimental results, we estimate that presented results are credible, despite the lack of experimental confirmation.

Acknowledgement
The research was partly funded by the Slovenian Research Agency ARRS - Contract No. 1000-09-160263.

References

[1] Sato T, Nagahara T, Tanaka K, Fuchiwaki M ans Shimizu F 2010 Vortex cavitation and oscillation in a double-suction volute pump *IOP Conf. Ser.: Earth Environ. Sci.* **12** 012019 (8pp)
[2] Gülich JF 2008 *Centrifugal Pumps* (Berlin: Springer)
[3] Škerlavaj A, Titzschkau M, Pavlin R, Vehar F, Mežnar P and Lipej A 2012 Cavitation improvement of double suction centrifugal pump HPP Fuhren *IOP Conf. Ser.: Earth Environ. Sci.* **15** 022009 (8pp)
[4] Ansys 2011 *Ansys CFX-Solver Theory Guide*
[5] Menter FR, Kuntz M and Langtry R 2003 Ten years of industrial experience with the SST turbulence model *Turbulence, Heat and Mass Transfer 4* eds. K Hanjalić, Y Nagano and M Tummers (New York: Begell House) pp 625-632
[6] Smirnov PE and Menter F 2009 Sensitization of the SST turbulence model to rotation and curvature by applying the Spalart-Shur correction term *J. Turbomach.* **131** 041010
[7] Vehar F, Škerlavaj A, Mežnar P, Pavlin R 2011 KW Fuhren – *Hydraulic development of improved impeller and inlet section* Report Nr. 3041 (Ljubljana: Turboinštitut) p 47
[8] Egorov Y and Menter F 2008 Development and application of SST-SAS turbulence model in the DESIDER project *Advances in Hybrid RANS-LES Modelling* eds. S-H Peng and W Haase (Heidelberg: Springer) pp 261–270
[9] Barth TJ and Jespersen DC 1989 The design and application of upwind schemes on unstructured meshes *Proc. of 27th Aerosp. Sci. Meet.* (Reno: AIAA) 0366 (12pp)
[10] Jasak H, Weller HG and Gosman AD 1999 High resolution NVD differencing scheme for arbitrarily unstructured meshes *Int. J. Numer. Meth. Fluids* **31**(2) pp 431-449
[11] Jeong J and Hussain F 1995 On the identification of a vortex *J. Fluid Mech.* **285** pp 69-94
[12] Škerlavaj A, Škerget L, Ravnik J and Lipej A 2011 Choice of a turbulence model for pump intakes *Proc. Inst. Mech. Eng. Part A: J. Power Energy* **225** pp 764-778

Nomenclature

Variables and quantities:

c	[m/s]	Absolute velocity
Q	[s^{-2}]	Second invariant of velocity gradient [10]
u	[m/s]	Tangential velocity of impeller at observed point
w	[m/s]	Velocity relative to impeller blade
Z	[m]	Cartesian coordinate
β	[°]	Angle between w and u

Indexes:

1	At impeller inlet

Abbreviations:

CR	Counter-rotating
DE	Drive-end
NDE	Non-drive-end
PR	Pre-rotating